LETTERS
PUBLISHED ONLINE: 22 DECEMBER 2014 | DOI: 10.1038/NCLIMATE2474
nature climate change

Barrier island bistability induced by biophysical interactions

Orencio Durán Vinent*† and Laura J. Moore

Barrier islands represent about 10% of the world's coastline[1], sustain rich ecosystems, host valuable infrastructure and protect mainland coasts from storms. Future climate-change-induced increases in the intensity and frequency of major hurricanes[2] and accelerations in sea-level rise[3,4] will have a significant impact on barrier islands[5,6]—leading to increased coastal hazards and flooding—yet our understanding of island response to external drivers remains limited[1,7,8]. Here, we find that island response is intrinsically bistable and controlled by previously unrecognized dynamics: the competing, and quantifiable, effects of storm erosion, sea-level rise, and the aeolian and biological processes that enable and drive dune recovery. When the biophysical processes driving dune recovery dominate, islands tend to be high in elevation and vulnerability to storms is minimized. Alternatively, when the effects of storm erosion dominate, islands may become trapped in a perpetual state of low elevation and maximum vulnerability to storms, even under mild storm conditions. When sea-level rise dominates, islands become unstable and face possible disintegration. This quantification of barrier island dynamics is supported by data from the Virginia Barrier Islands, USA and provides a broader context for considering island response to climate change and the likelihood of potentially abrupt transitions in island state.

Barrier islands respond to rising sea level by migrating landward or drowning[7,9,10]. Landward migration is driven mostly by storms and is controlled by island elevation. Extensive measurements of dune elevation performed at the Virginia Barrier Islands[11], a relatively undisturbed barrier system including 12 islands, show a bimodal distribution of barrier island elevation with two well-defined island types: low-elevation and high-elevation islands (Fig. 1 and Supplementary Fig. 1). Low islands lacking vegetated dunes are relatively narrow and prone to frequent overwash, resulting in rapid landward migration (Fig. 1a,b,g) and low biodiversity (as in the case of the islands associated with the Mississippi Delta, for example, the Chandeleur Islands). In contrast, high islands with well-developed dunes resist storm impacts, are wider and migrate slowly (if at all, Fig. 1c,d,g) and support a rich ecosystem and/or human development. In this way, barrier island evolution is fundamentally linked to dune dynamics. However, because vegetated dunes both protect islands from storm impacts and are themselves eroded by storms and affected by rising sea level, island dynamics ultimately arise from the competition between dune erosion and dune formation.

We investigate this competition by adding the effects of storms and sea-level rise into a model of the physical and biological processes involved in coastal dune formation[14], and then simulating long-term barrier island dynamics as multiple cycles of dune formation alternating with dune erosion during high water events (HWEs; including all events—arising from local and distant storms—in which total water level R, that is, mean sea level + tides + storm surge + wave run-up, is above the mean high water level (MHWL)). The resulting model consists of a set of differential equations describing the morphodynamic feedback between aeolian sand transport and topography, the interaction between vegetation growth and sand transport, and the effects of the shoreline on sand transport, as well as the newly added effects of vegetation sensitivity to saltwater inundation[15,16], storm-induced sand transport above MHWL, and relative sea-level rise (RSLR; Methods and Supplementary Methods). For simplicity all boundary and initial conditions are uniform in the alongshore direction (that is, the island has alongshore symmetry) and thus, island elevation is equivalent to local dune elevation.

Simulations show that immediately following an overwash event, island elevation is too low to sustain the growth of 'dune-building' plants (Fig. 2a). In the absence of vegetation, small non-vegetated dunes slowly nucleate at the back of the beach in response to the interaction between morphology and wind flow (Fig. 2c and Supplementary Fig. 2) following the same mechanisms as the nucleation of desert dunes[17]. Once sand elevation is sufficiently high to allow vegetation recovery (a threshold defined by the minimum elevation Z_c above the MHWL that 'dune-building' plants can effectively grow, see Methods) vegetated dune growth begins as plants trap sand, thereby accelerating vertical accretion and leading to rapid dune building. In the absence of storm erosion, dunes eventually reach a maximum size[14] (Fig. 2a,b).

Consideration of the processes behind vegetation recovery, and thus dune recovery, shows that the vegetation recovery time T_v increases with RSLR because the rate of net surface accretion—which prevents frequent saltwater inundation of the backshore and leads to vegetation recovery—is the difference between the growth rate G_0 of the non-vegetated incipient dunes and the rate S of RSLR. The growth rate G_0 scales as the ratio of the mean aeolian sand flux at the beach q_0, an increasing function of wind intensity and (dry-) sand supply, and the non-vegetated dune wavelength λ (ref. 17). The vegetation recovery time T_v then relates the primary factors influencing vegetation and dune recovery: vegetation sensitivity to inundation (Z_c), aeolian transport (q_0) and RSLR (S): $T_v \approx Z_c/(\beta q_0 \lambda^{-1} - S)$, with fitting parameter $\beta \approx 0.1$ (Supplementary Fig. 3).

After imposing periodic HWEs with random total water level R, the stochastic dynamics of barrier island elevation is controlled by the ratio of the vegetation recovery time (T_v) and the period (T_{HWE}) of HWEs (Fig. 3a–c). This ratio characterizes the competition between external erosive and internal recovery processes and therefore we call it the 'vulnerability' index ($\gamma = T_v/T_{HWE}$). When the period of HWEs is larger than the vegetation recovery time ($\gamma < 1$), vegetation recovers before the next HWE, thus enabling rapid dune growth (Fig. 3a). As dune erosion is mainly controlled by

University of North Carolina, Department of Geological Sciences, 104 South Rd, Mitchell Hall, Campus Box 3315, Chapel Hill, North Carolina 27515, USA.
†Present address: MARUM-Center for Marine Environmental Sciences, University of Bremen, Leobener Str., D-28359 Bremen, Germany.
*e-mail: oduran@marum.de

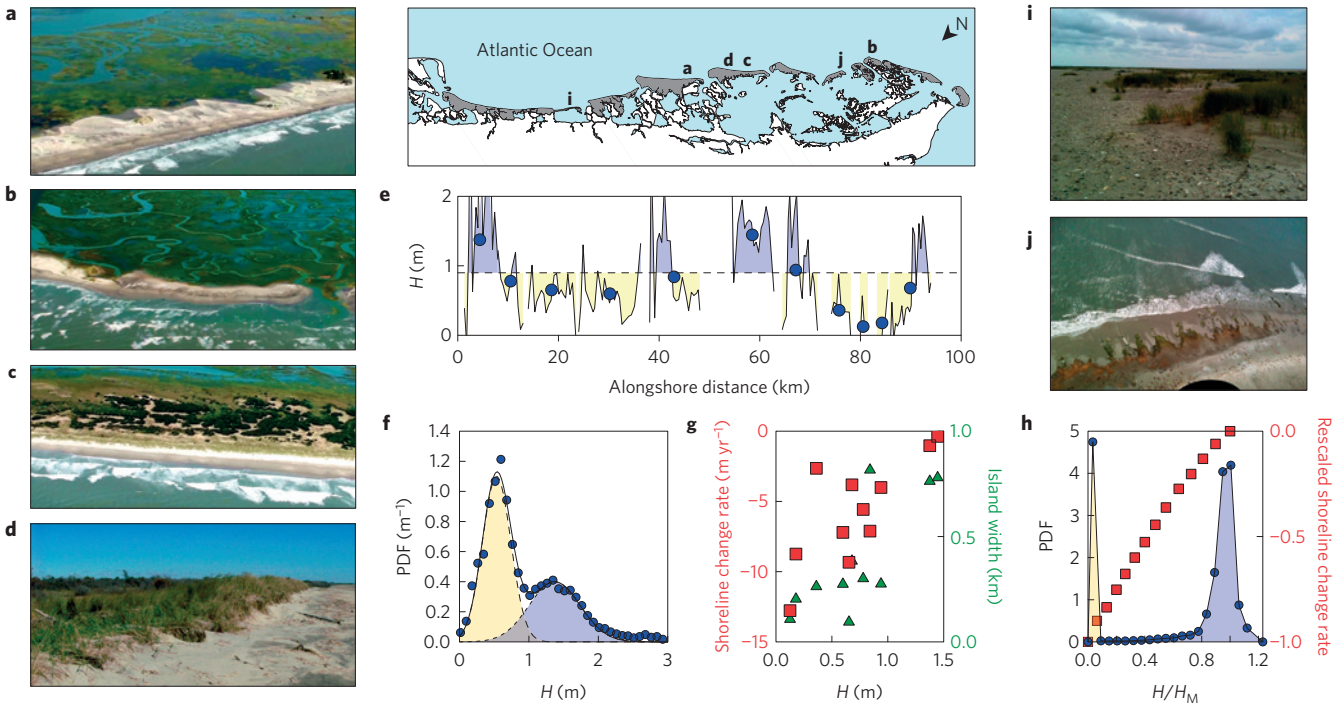

Figure 1 | Empirical evidence for barrier island bistability. a–d, Examples of low (**a**,**b**) and high (**c**,**d**) barrier islands, that is, islands without and with well-developed dunes, along the Virginia Barrier Islands, US mid-Atlantic coast (included map): Paramore (**a**), Myrtle (**b**) and Hog (**c**,**d**). **e**, Alongshore island elevation (elevation of primary dune relative to beach berm)[11] derived from 2005 lidar data (solid line) and average island elevation (filled circles). **f**, Probability density function (PDF) of measured elevations (symbols) with best fit by a bimodal normal distribution (lines). The crossover elevation is used to define high (blue) and low (yellow) regions in **e**. **g**, Average island shoreline change rate (squares), used as a proxy for island migration, and island width (triangles), as function of average island elevation H. Shoreline change rates are calculated from shoreline positions in the period 1945–2005 (ref. 12) and island widths are calculated from reported data on island area[13]. **h**, PDF of simulated island elevations (circles) and simulated shoreline change rate (squares) rescaled by the value at the low state, as function of the average island elevation. Simulations were performed for $\gamma = 1.5$. **i**,**j**, Photos illustrate shell armouring (**i**) and the exposure of marsh platform on the foreshore (**j**) at the two low-elevation locations noted by corresponding symbols in the map.

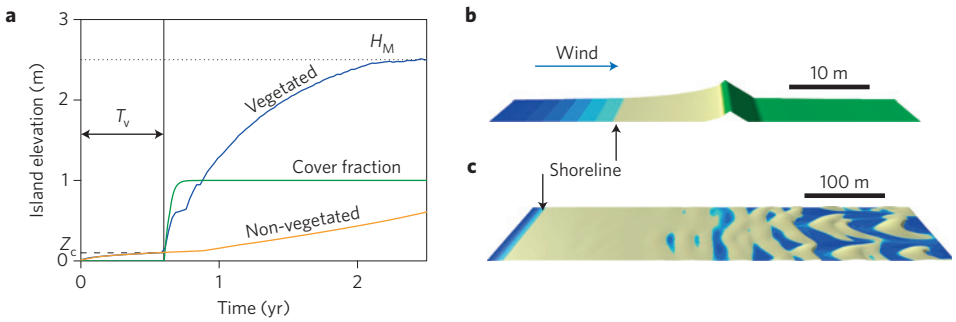

Figure 2 | Post-storm barrier island recovery. a, Post-storm evolution of island elevation (with and without vegetation) and vegetation cover fraction. H_M is the maximum vegetated dune elevation, T_v is the vegetation recovery time and Z_c is the vegetation sensitivity to saltwater inundation. **b**,**c**, Simulated steady state for coastal dunes with (**b**) and without (**c**) vegetation. Dry-sand areas are yellow, vegetation is green and intertidal areas (that is, below MHWL) are blue.

the ratio between R and dune elevation H (ref. 18; Supplementary Fig. 4), rapid dune recovery leads to a negative feedback in which higher elevation, and therefore lower vulnerability to wave erosion, allows dunes to remain close to their maximum height. This high-elevation state thus represents a stable dynamical equilibrium for barrier island elevation. When the period of HWEs is shorter than the vegetation recovery time ($\gamma > 1$), low areas devoid of vegetation cannot recover before the next HWE. They remain vulnerable to erosion and are thus kept in a low-elevation state. In contrast, well-developed dunes are less prone to overwash and even when partially eroded—as long as some elevation and vegetation remain—they can recover quickly, evolving towards the high-elevation state. Therefore, for $\gamma > 1$ there is a tendency for a barrier island to exist either as a stable high island or a stable low island and the island becomes bistable (Fig. 3b,c). The onset of the bistable behaviour at $\gamma = 1$ has been verified numerically for varying winds, rates of RSLR and vegetation sensitivities (Fig. 3d,e).

The predicted bistability of island dynamics offers an explanation for the bimodal probability distribution function of island elevation observed for the Virginia Barrier Islands, along the mid-Atlantic coast of the US. Assuming the temporal randomness of HWEs impacting a given location of the island is equivalent to the spatial randomness of HWEs acting at different locations alongshore, it is possible to compare qualitatively the simulated time series of local

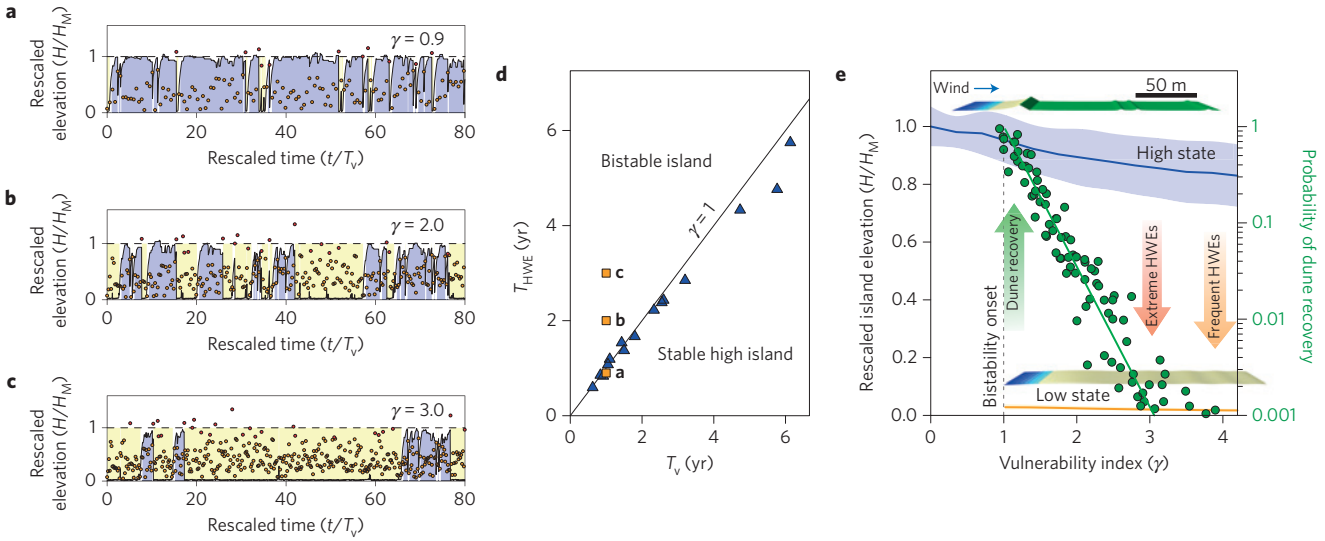

Figure 3 | Bistability of island elevation. a–c, Evolution of the rescaled dune elevation H/H_M under a series of HWEs with period $T_{HWE} = \gamma T_v$, for $\gamma = 0.9$ (**a**), 2 (**b**) and 3 (**c**). γ is the vulnerability index and T_v is the vegetation recovery time. Symbols represent rescaled total water level R/H_M. Red symbols denote extreme events (that is, those leading to overwash). Elevations above $0.8H_M$ (high state) and below $0.2H_M$ (low state) are highlighted in blue and yellow, respectively. **d**, Onset of bistability calculated from model runs for different parameters (triangles). Squares represent the particular cases shown in **a–c**. Solid line: predicted bistability onset represented by the condition $T_{HWE} = T_v$ ($\gamma = 1$). **e**, Equilibrium states for island elevation and probability of dune recovery (green symbols) as a function of γ, for varying winds, rates of RSLR and vegetation sensitivities (see Methods for range of parameter values used). Green line corresponds to the exponential fit $a^{\gamma-1}$ ($a = 0.035$) for the recovery probability (defined as the inverse of the average number of HWEs spent in the low state). Blue and orange lines are the average values for the stable high and low equilibrium respectively, and the shadow area on either side of the line represents the data dispersion. The onset of bistability, which occurs when the probability of dune recovery decreases below 1 (dashed line), and the processes leading to a transition between alternative states (arrows) are shown for reference. In the snapshots of simulated high and low islands, dry-sand areas are yellow, vegetation is green and intertidal areas (that is, below MHWL) are blue.

island elevation (for example, Fig. 2b) to the measured alongshore elevation (Fig. 1e). In addition to predicting the observed bimodal distribution of dune elevation (Fig. 1f), the model also reproduces increases in shoreline change rate (used as a proxy for island migration rate) with decreasing average island elevation (Fig. 1g,h), which can be understood as an increasing contribution to average island migration rates from the rapidly migrating low sections of the island.

Within the bistable regime the stochastic nature of HWEs allows barrier islands to explore alternative equilibrium states with a certain probability. Transition from a high to a low state can be triggered either by low-frequency high-energy events such as large storms, or by frequent medium-energy events (Fig. 3a–c and Supplementary Fig. 5). As the conditions to sustain a mature vegetated dune are very different from those needed to build it in the first place, there is a hysteresis in the response of island elevation to changing conditions, with dune recovery taking place at a lower vulnerability index than the one required for severe dune erosion (Supplementary Fig. 5a). Therefore, the fact that an island is in a high state is not enough to conclude that it can recover quickly once in the low state, as can be seen in Fig. 3b,c where dune recovery takes longer for increasing vulnerability indices. Indeed, simulations show that the probability of dune, and therefore island, recovery (that is, of entering the attractive basin of the high state) decreases exponentially with the vulnerability index (Fig. 3e), which means that the island will remain low in elevation for exponentially longer times.

The vulnerability index, which can be rewritten using the scaling of the vegetation recovery time as

$$\gamma = Z_c T_{HWE}^{-1} / (\beta q_0 \lambda^{-1} - S) \quad (1)$$

summarizes the role of the key factors driving barrier island response (Fig. 4). The transition from a stable high island to a bistable one is accelerated by higher rates of RSLR, more vulnerable vegetation or more frequent HWEs, but retarded by increasing aeolian transport. For negative net accretion rates ($\gamma < 0$) the island enters a new unstable regime in which the low-elevation state becomes intertidal/subtidal (that is, below the MHWL) and the island may disintegrate (Fig. 4). Therefore, the vulnerability index provides a deeper insight into long-term island dynamics, regardless of perturbations that may occur in the short term. For example, the progressive disintegration of barrier islands along the Mississippi Delta (for example, the Chandeleur Islands) that has been attributed to a series of recent major storms[20] could alternatively be understood as a consequence of transition into the unstable regime (Fig. 4) triggered by an increase in RSLR compounded by a reduction in sand supply[9]. Similarly, the Virginia Barrier Islands seem to have experienced transition to the bistable regime, in which high and low islands coexist, possibly driven by locally high RSLR (ref. 4) and a reduction in aeolian sand transport arising from the combined effects of shell armouring[21] and exposure of marsh platform (that is, less sand supply) on the foreshore (Fig. 1i,j).

The bistable dynamics suggested by model results contributes to a growing literature reporting the existence of alternative stable states in ecosystems as diverse as arid lands, forests, lakes, oceans and coral reefs[22] and more recently, shallow coastal bays[23]. Along with a few more recent studies[24,25], we demonstrate the importance of biophysical feedbacks in leading to state changes that affect not only the ecosystem that inhabits the landscape, but the morphology of the landscape itself. As in all multi-state systems, barrier islands—which are often heavily developed, and which serve as important interfaces between the marine and terrestrial realms—may cross the threshold to bistability silently, without providing observable evidence until the state change becomes locked in place by a random event. In addition, because barrier islands are coupled to adjacent coastal ecosystems such as shallow coastal bays and marshes[26], which also exhibit multiple stable states[23], a disturbance that triggers a transition in island state may initiate a cascade of transitions across

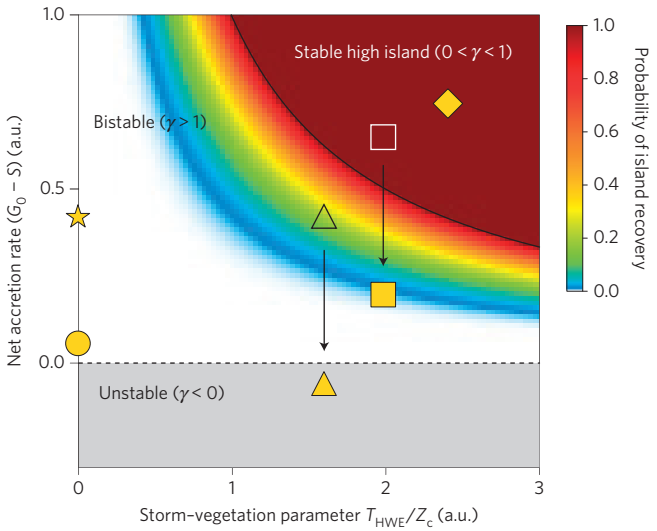

Figure 4 | Dynamical states and transitions. Barrier island response, in terms of the vulnerability index γ, as function of the net aeolian accretion rate (G_0–S), where $G_0 = \beta q_0 \lambda^{-1}$, and the storm–vegetation parameter $T_{HWE} Z_c^{-1}$ (equation (1)) in arbitrary units (a.u.). S is the rate of RSLR, q_0 is the average aeolian sand flux, Z_c is the minimum elevation above MHWL that vegetation can grow, λ is the wavelength of the non-vegetated incipient dunes, T_{HWE} is the period of HWE and β is a fit parameter. The probability of dune, and therefore island, recovery (Fig. 3e) is shown in colours. Solid and dashed lines represent the onset of bistability and the transition to a potentially unstable barrier island (grey area), respectively. Circle: non-vegetated low islands with low aeolian sand transport (for example, Alaska Barrier Islands[1]), star: non-vegetated low islands having especially active aeolian sand transport (for example, Baja California, Mexico), diamond: stable high islands (for example, the central two-thirds of 40-km-long Sable Island, Newfoundland[19]). Arrows represent suggested transitions taking place at the Chandeleur Islands, Louisiana, US (triangles) and at the Virginia Barrier Islands, Virginia, US (squares). Open (filled) symbols represent suggested past (present) condition. The absence of vegetation is given by the limit $Z_c \to \infty$.

the broader landscape. For landscapes and ecosystems generally, analytical expressions for boundaries between system regimes (for example, from stable to bistable, or from bistable to unstable) have the potential to be even more useful than leading indicators[27] that merely warn of an impending change. For example, control parameters such as the vulnerability index have the potential to provide a means for assessing the likelihood that a landscape system will transition to a new regime under a given set of conditions, as well as quantitative guidance on management strategies intended to decrease system vulnerability and increase resilience.

Methods

The coastal dune model describes the temporal evolution of the sand surface elevation $h(x,y,t)$—defined relative to the MHWL—and the cover fraction $\rho_{veg}(x,y,t)$ for a single generic grass species. x is the cross-shore distance to the shoreline ($x=0$), which separates the foreshore ($x<0$) from the backshore ($x>0$), and y is the alongshore coordinate. A complete description of the coastal dune model is provided in the Supplementary Methods and includes further details on the calculation of the aeolian transport and vegetation dynamics as well as the initial and boundary conditions used to integrate the model.

Aeolian sand transport. In the absence of storms, the sand flux $\mathbf{q}_a(x,y,t)$ is calculated from the bed wind shear stress, which depends on the surrounding topography and the vegetation cover, and the local sand transport threshold, which we assume is primarily controlled by the sand moisture content. For simplicity in the formulation, sand transport is described by volume, not mass, flux.

Storms. Storms are defined in the model as HWEs with total water elevation R above the MHWL (R is defined relative to the MHWL). HWEs are considered periodic with period T_{HWE} and have constant duration. R is randomly distributed following an Erlang distribution $R^2 \bar{R}^{-3} e^{-3R/\bar{R}}$ ($\bar{R}$ is mean total water elevation), which has an exponential tail, in agreement with ref. 28, and filters tidal events (that is, there are no events for $R \to 0$).

Storm-induced sand transport. We derive a phenomenological expression to calculate the cross-shore sand flux $q_{st}(x,y,t)$ for elevations between MHWL and R during HWEs. On the basis of ref. 29 (see ref. 30 for the validation of a similar formulation), we assume the net sand flux q_{st} over many swash cycles is proportional to the cube of the average speed U of the uprushing wavefront, times the time δt this particular location is submerged: $q_{st} \propto U^3 \delta t/(gT)$, with gravity g and timescale T. The net sand flux is weighted by a downslope contribution $(1-\partial_x h/\tan(\alpha))$ that represents the tendency of the surface to reach the equilibrium foreshore slope $\tan(\alpha)$. From energy conservation, the kinetic energy of the uprushing wavefront is approximately balanced by its potential energy. In this case $U \propto \sqrt{g(R-h)}$ and $\delta t \propto \sqrt{g(R-h)}$ (ref. 29), which leads to

$$q_{st} = T^{-1}(R-h)^2(1-\partial_x h/\tan(\alpha))$$

We choose the rescaled duration of HWEs to qualitatively reproduce the main erosional regimes described in ref. 18 (Supplementary Fig. 4). Crucially, the predicted bistable behaviour of barrier islands depends only on the existence of these erosional regimes and not on the details of the sand flux formulation.

Surface dynamics. At the foreshore ($x<0$), we assume an equilibrium defined by a constant slope of angle α. This assumption implies that aeolian erosion is balanced by accretion in the swash zone. As a result, the simulated foreshore acts as a sand reservoir supplying an unlimited amount of sediment to the backshore, effectively feeding dune formation and post-storm recovery. For the shoreline ($x=0$), we assume, as a first approximation, that under RSLR it follows Bruun's rule and migrates landward at a rate $\dot{x}_{shore}$ proportional to the rate S of RSLR. At the backshore ($x>0$), we calculate the change in the sand surface elevation h from mass conservation as

$$\partial h/\partial t = -\partial q_{st}/\partial x$$

during HWEs, and

$$\partial h/\partial t = -\nabla \cdot \mathbf{q}_a S + \dot{x}_{shore} \partial h/\partial x$$

otherwise. The last two terms at the right-hand side describe the effects of RSLR and appear because we define the surface elevation relative to the sea level and the shoreline position.

Vegetation dynamics. As a first approximation, we assume a single generic grass species with a cover fraction ρ_{veg} that is sensitive to sand erosion and accretion and that can increase up to the maximum cover $\rho_{veg}=1$ during a characteristic time t_{veg}. We further assume plant growth is also sensitive to frequent saltwater inundation and thus to the proximity of the shoreline and to the elevation above MHWL, such that plants can effectively grow only landward of the vegetation limit L_{veg} and in places higher than a minimum elevation Z_c. Thus,

$$\mathrm{d}\rho_{veg}/\mathrm{d}t = (1-\rho_{veg}) t_{veg}^{-1} \Theta(x-L_{veg}) \Theta(h-Z_c) - 1m^{-1} |\partial h/\partial t|$$

where the Heaviside function $\Theta(s)$ (1 for $s>0$; 0 otherwise) defines the regions where plants can grow.

Parameters. We investigate model outcomes as function of the parameters characterizing the external forcing and the response of the system (the explored range is in parenthesis): the vertical vegetation limit Z_c (0.02–0.2 m), frequency of HWEs T_{HWE} (0–20 yr), mean total water elevation $\bar{R}$ (1–2 m), rate S of RSLR (0–0.02 m yr^{-1}) and the imposed onshore wind, characterized by the ratio of the undisturbed shear velocity u_{*0} and the transport threshold u_t (1.5–2.5), and by the fraction r_t of the time the wind is above the transport threshold and sand is available.

Received 6 June 2014; accepted 19 November 2014; published online 22 December 2014

References

1. Stutz, M. L. & Pilkey, O. H. Open-ocean barrier islands: Global influence of climatic, oceanographic, and depositional settings. *J. Coast. Res.* **272,** 207–222 (2011).

2. Emanuel, K. Downscaling CMIP5 climate models shows increased tropical cyclone activity over the 21st century. *Proc. Natl Acad. Sci. USA* **110,** 12219–12224 (2013).
3. IPCC *Climate Change 2014: Impacts, Adaptation and Vulnerability* (Cambridge Univ. Press, 2014).
4. Sallenger, A. H., Doran, K. S. & Howd, P. A. Hotspot of accelerated sea-level rise on the Atlantic coast of North America. *Nature Clim. Change* **2,** 884–888 (2012).
5. McNamara, D. E. & Keeler, A. A coupled physical and economic model of the response of coastal real estate to climate risk. *Nature Clim. Change* **3,** 1–4 (2013).
6. Woodruff, J. D., Irish, J. L. & Camargo, S. J. Coastal flooding by tropical cyclones and sea-level rise. *Nature* **504,** 44–52 (2013).
7. FitzGerald, D. M., Fenster, M. S., Argow, B. A. & Buynevich, I. V. Coastal impacts due to sea-level rise. *Annu. Rev. Earth Planet. Sci* **36,** 601–647 (2008).
8. Cazenave, A. & Le Cozannet, G. Sea level rise and its coastal impacts. *Earth's Future* **2,** 1–20 (2013).
9. Blum, M. D. & Roberts, H. H. Drowning of the Mississippi Delta due to insufficient sediment supply and global sea-level rise. *Nature Geosci.* **2,** 488–491 (2009).
10. Moore, L. J., List, J. H., Williams, S. J. & Stolper, D. Complexities in barrier island response to sea level rise: Insights from numerical model experiments, North Carolina Outer Banks. *J. Geophys. Res.* **115,** F03004 (2010).
11. Oster, D. *The Influence of Morphology on Barrier Island Recovery Following Storms: Insights from The Virginia Barrier Islands, Mid-Atlantic Bight* Master's thesis, Univ. Virginia (2012).
12. Johnson, J. *Geomorphic Consequences of Wave Climate Alteration along Cuspate Coastlines* Master's thesis, Univ. North Carolina (2013).
13. Young, D., Porter, J. & Bachmann, C. Cross-scale patterns in shrub thicket dynamics in the Virginia barrier complex. *Ecosystems* **10,** 854–863 (2007).
14. Durán, O. & Moore, L. J. Vegetation controls on the maximum size of coastal dunes. *Proc. Natl Acad. Sci. USA* **110,** 17217–17222 (2013).
15. Barbour, M., Jong, T. & Pavlik, B. in *Physiological Ecology of North American Plant Communities* (eds Chabot, B. & Mooney, H.) 296–322 (Springer, 1985).
16. Huiskes, A. Biological flora of the British Isles: *Ammophila arenaria* (L.) Link (*Psamma arenaria* (L.) Roem. et Schult.; *Calamgrostis arenaria* (L.) Roth). *J. Ecol.* **67,** 363–382 (1979).
17. Elbelrhiti, H., Claudin, P. & Andreotti, B. Field evidence for surface-wave-induced instability of sand dunes. *Nature* **437,** 720–723 (2005).
18. Sallenger, A. H. Storm impact scale for barrier islands. *J. Coast. Res.* **16,** 890–895 (2000).
19. Byrne, M-L. & McCann, S. B. The dunescape of sable island. *Can. Geogr.-Geogr. Can.* **39,** 363–368 (1995).
20. Fearnley, S. M., Miner, M. D., Kulp, M., Bohling, C. & Penland, S. Hurricane impact and recovery shoreline change analysis of the Chandeleur Islands, Louisiana, USA: 1855 to 2005. *Geo-Mar. Lett.* **29,** 455–466 (2009).
21. Wolner, C. W. V. *et al.* Ecomorphodynamic feedbacks and barrier island response to disturbance: Insights from the Virginia Barrier Islands, Mid-Atlantic Bight, USA. *Geomorphology* **199,** 115–128 (2013).
22. Scheffer, M., Carpenter, S., Foley, J. A., Folke, C. & Walker, B. Catastrophic shifts in ecosystems. *Nature* **413,** 591–596 (2001).
23. McGlathery, K. J., Reidenbach, M. A., D'Odorico, P. D., Fagherazzi, S. & Porter, J. H. Nonlinear dynamics and alternative stable states in shallow coastal systems. *Oceanography* **26,** 220–231 (2013).
24. Fagherazzi, S., Carniello, S. L., D'Alpaos, L. & Defina, A. Critical bifurcation of shallow microtidal landforms in tidal flats and salt marshes. *Proc. Natl Acad. Sci. USA* **103,** 8337–8341 (2006).
25. Marani, M., Da Lio, C. & D'Alpaos, A. Vegetation engineers marsh morphology through multiple competing stable states. *Proc. Natl Acad. Sci. USA* **110,** 3259–3263 (2013).
26. Walters, D., Moore, L. J., Durán, O., Fagherazzi, S. & Mariotti, G. Interactions between barrier islands and backbarrier marshes affect island system response to sea level rise: Insights from a coupled model. *J. Geophys. Res.* **119,** 2013–2031 (2014).
27. Scheffer, M. *et al.* Early-warning signals for critical transitions. *Nature* **451,** 53–57 (2009).
28. Ruggiero, P., Komar, P. D., McDougal, W. G., Marra, J. J. & Beach, R. A. Wave runup, extreme water levels and the erosion of properties backing beaches. *J. Coast. Res.* **17,** 407–419 (2001).
29. Larson, M., Kubota, S. & Erikson, K. Swash-zone sediment transport and foreshore evolution: Field experiments and mathematical modeling. *Mar. Geol.* **212,** 61–79 (2004).
30. Larson, M., Wise, R. A. & Kraus, N. C. *Coastal Overwash, Part 2: Upgrade to SBEACH, ERDC/RSM- TN-15* (US Army Engineer Research and Development Center, 2004).

Acknowledgements

Financial support was provided by the Virginia Coast Reserve Long-Term Ecological Research Program (National Science Foundation DEB-123773), the Department of Energy's Office of Science through the Coastal Center of the National Institute for Climatic Change Research at Tulane University, the Geomorphology and Land use Dynamics Program of the National Science Foundation (EAR-1324973), and the University of North Carolina at Chapel Hill. The authors are grateful to A. B. Murray (Duke University), P. Haff (Duke University) and J. Bruno (University of North Carolina-Chapel Hill) for helpful feedback on this manuscript before submission.

Author contributions

Both authors contributed extensively to this work.

Additional information

Supplementary information is available in the online version of the paper. Reprints and permissions information is available online at www.nature.com/reprints. Correspondence and requests for materials should be addressed to O.D.V.

Competing financial interests

The authors declare no competing financial interests.